Journal of Industrial and Engineering Chemistry 54 (2017) 59–68

Contents lists available at ScienceDirect

Journal of Industrial and Engineering Chemistry

journal homepage: www.elsevier.com/locate/jiec

Development of amine-functionalized hierarchically porous silica for CO_2 capture

Guojie Zhang*, Peiyu Zhao, Ying Xu

Key Laboratory of Coal Science and Technology, Ministry of Education and Shanxi Province, Taiyuan University of Technology, Taiyuan 030024, PR China

ARTICLE INFO

Article history:
Received 3 February 2017
Received in revised form 14 April 2017
Accepted 14 May 2017
Available online 22 May 2017

Keyword:
Amine impregnated
Nanosilicon
CO_2 capture
Regenerability

ABSTRACT

A kind of hierarchical porous silica (HPS) was synthesized in a relatively mild condition and then devoted as the supports to fabricate TEPA-impregnated adsorbents for CO_2 adsorption. HPS has different pore size distribution and the huge pore volume. These structure characteristics of HPS can mitigate the mass transfer resistance which occurs more serious in traditional carrier materials with single smaller channel. The CO_2 adsorption performances of modified HPS were investigated in a homemade fixed bed reactor under different conditions. The HPS exhibited maximum CO_2 adsorption capacities of 5.01 mmol/g when 60 wt.% TEPA loaded. It presented better TEPA loading properties and higher CO_2 adsorption capacities than the majority of the single ordered mesoporous adsorbents according to the literature. When the adsorption experiments were repeated ten times, the amount of CO_2 capture reduces from 5.01 mmol/g to 4.7 mmol/g, only 6.1% reduction. And the deactivation model which can describe the absorption of CO_2 was adopted under different experiment conditions. In all these cases, the experimental data of CO_2 adsorption gave a good agreement with the predicted results by the breakthrough model.

Introduction

Carbon dioxide is considered as the most important greenhouse gas, and the combustion of fossil fuels (coal, petroleum and natural gas) is the main source of carbon dioxide emission [1,2]. Hence, the capture of CO_2 from factory combustion flue gas is regarded as the most effective way to reduce the effect of global warming [3,4]. Many traditional technologies for CO_2 capture have been developed, for example, chemical adsorption of amine solution. This method has the advantage of low price and high CO_2 absorption capacity [5,6]. But, the amine solution for CO_2 capture also has many shortcomings, such as the toxic, flammable, corrosive, and the high regeneration energy. These inherent drawbacks make a bottleneck for industrial applications [7]. Therefore, it is also a challenge to develop a more efficient CO_2 adsorbent for researchers all over the world.

For the liquid phase absorption, solid adsorbents for CO_2 capture are a promising alternative technology. The solid adsorbents have the advantage of energy savings and stable performance by using of the change of pressure or temperature [8,9]. Under normal circumstances, porous materials such as zeolites [10–13], activated carbons [14,15], mesoporous silica [16–18], metal oxides [19,20], metal organic frameworks [21,22], can be used for CO_2 capture. The CO_2 was captured by physical adsorption induced by either ion-quadrupole interaction or van der Waals force [23]. However, the CO_2 adsorption capacity decreased faster at high temperature. Meanwhile, these materials have the disadvantage of lower selectivity and water tolerance [24].

Recently, solid amine adsorbents developed by amines species loaded on certain carrier materials are widely investigated [25–27]. Compared with the liquid phase absorption, these solid amine adsorbents usually need lower capital cost and less energy for regeneration of adsorbents. In addition, the equipment corrosion problems also can be resolved which usually observed in the process of the liquid phase amine absorption. The solid amnie adsorbents can be prepared either by grafting with different amine species covalently bound to the support [28] or physical wet impregnation with polyethylenimine (PEI), tetraethylenepentamine (TEPA) dissolved in an organic solvent [29].

Following the first report of amine supported on MCM-41 [30], many porous silica materials, such as MCM-41 [31], SBA-15 [32], have been afforded as amines supports for CO_2 recovery. For these

* Corresponding author.
E-mail addresses: zhgjdoc@126.com, zhangguojie@tyut.edu.cn (G. Zhang).

http://dx.doi.org/10.1016/j.jiec.2017.05.018
1226-086X/

amine modified solid adsorbents, amines can be loaded into the carrier channel leading to the better dispersion of amines, which makes contribute to the improvement of CO_2 adsorption capacity. However, these solid amine adsorbents still have some shortcomings, especially with respect to the carrier materials. First, there is a relatively small pore volume (only about 1 cm^3/g) for these ordered mesoporous silica carrier. The loading amount of amine species and CO_2 adsorption were both limited [33]. Second, these silica carrier materials have only simple mesoporous. These simple channels are easily blocked by amines chains, which increase the kinetic barrier for CO_2 diffusion and reduce the mass transfer rate in process of CO_2 capture [34].

Compared with simple mesoporous silica materials, we noticed that hierarchical pore silica which possess a special structure with different pore size distribution [35–37]. The hierarchical pore structure and larger pore volume of this carrier make it possible to enhance amines loading capacity and provide easier access to the active sites. And the mass transfer rate of CO_2 in the adsorption–desorption process was also increased. Therefore, the adsorbents with hierarchical pore structure would facilitate high CO_2 adsorption capacity and high CO_2 adsorption rate at the same time.

In this work, we synthesized the hierarchical porous silica (HPS) in a relatively mild condition. Then the hierarchical porous silica was devoted as the supports to fabricate TEPA-impregnated adsorbents for CO_2 adsorption. The physical characteristics (e.g., pore structure, pore volume) of the support and CO_2 adsorption performances of the adsorbents were investigated under different conditions (e.g., adsorption temperatures, amine loading capacity). The HPS composite adsorbent with high amine loading of 60 wt% shows a large capacity up to 5.01 mmol/g at 75 °C under simulated flue gas conditions (15 vol.% CO_2) by the CO_2 adsorption tests which performed in a fixed-bed reactor. In addition to their remarkable CO_2 capture capacity, this composite adsorbent also shows excellent stability and regenerability.

Experimental

Materials

Cetyltrimethy-lammonium bromide (CTAB), tetraethyl orthosilicate (TEOS, AR), polyethyleneglycol (PEG,Mw = 400), tetraethylenepentamine (TEPA, 90 wt%) and anhydrous ethanol solvent was purchased from Taiyuan Chemical (Taiyuan, China). Carbon dioxide (99.999%) and nitrogen (99.999%) were purchased from LiFeng Chemical Reagent (Taiyuan, China).

Synthesis of support

The hierarchical porous silica materials which have different pore distribution were prepared according to the methods provided by Loganathan et al. [38]; 18 ml PEG was dissolved in 120 ml deionized water and stirred for 10 min using a magnetic stirrer to form a clear solution at 40 °C. Then, 10 ml TEOS was drop wised into the solution under vigorous stirring, followed by the addition of 2 g CTAB under stirring. Then the gel mixture was generated after 2 ml aqueous ammonia was added. The gel mixture was isolated from the air to keep from the loss of ammonia. After the gel mixture was stirred at 40 °C for 12 h, the material was filtered and washed with the ethanol and deionized water, dried at 80 °C overnight. Then, the material was calcined at 550 °C for 6 h in air to remove the template.

The MCM-41 carrier was synthesized according to the methods provided in the literature [39]. 8.8 g template agent (CTAB) was dissolved in 200 ml deionized water at 40 °C. After CTAB was completely dispersed, 100 ml aqueous ammonia was introduced. In the state of continuing agitation, 20 ml Silicon source (TEOS) was dropwise in the above solution. Then the gel mixture was generated. The mixture was stirred constantly for 24 h and transferred to a Teflon-line steel autoclave and heated to 100 °C for 24 h. Then, the solid liquid mixture was filtered with the deionized water and ethanol, dried at 80 °C overnight, and finally calcined at 550 °C for 6 h in flowing air.

Preparation of amine-functionalized sorbents

The TEPA-impregnated adsorbents were developed by using of a typical impregnation method [29]. A certain amount of TEPA was dissolved in 20 ml of methanol at room temperature with magnetic stirring for 20 min, then 1 g of the porous carrier was introduce to the above mixture and further magnetic stirred forwards the slurry mixture generated. Then, the adsorbents was obtained by the slurry mixture was dried at 85 °C for 12 h. The sorbents was designated as HPS-TEPA-x, MCM-41-x, where x stands for the different load mass fractions of TEPA in sorbents. The calculation method of x is given by Eq. (1).

$$x = \frac{m_{TEPA}}{m_{TEPA} + m_0} \times 100\% \quad (1)$$

where m_{TEPA} is the added TEPA weight, g; m_0 is the carrier weight, g.

Characterization

Scanning electron microscopy (SEM, FEI Q-300) and transmission electron microscopy (TEM, JEOL 2010) were used to observe the samples morphology. The isotherm of adsorption-desorption was obtain at −196 °C by using of the principle of physical adsorption of N_2. Before N_2 adsorption–desorption test, the adsorbents were vacuum-treated for 4 h at 100 °C. The specific surface area of these samples was determined using the BET model. The total pore volume was estimated from the adsorbed capacity of N_2 at a relative pressure of $P/P_0 = 0.96$. The distribution of pore size was obtained through the BJH model for desorption branches of the isotherms. Fourier transform infrared (FTIR) was utilized to analysis the functional groups characteristic of the sample. The samples were firstly mixed and milled with KBr, and the spectra was recorded in the range of 400–4000 cm^{-1}. The XRD patterns of the samples were performed using a Rigaku diffractometer with Cu Kα (λ = 0.154 nm) radiation source. In situ IR DRIFTs (diffuse reflectance infrared Fourier transform spectroscopy, Thermo Scientific) used for CO_2 adsorption. The inlet gases were controlled by flow monitor and switched through a 4-port valve. Solid adsorbent was filled in the DRFITS with 80 mg. The IR cells was placed inside of FTIR (BrukerV70). The spectra was recorded in the range of 400–4000 cm^{-1}, the adsorbent was scanned once every 20 s.

Carbon dioxide adsorption/desorption teat

CO_2 adsorption/desorption tests were performed at atmospheric pressure in a homemade fixed-bed reactor (Fig. 1). 2.0 g of adsorbent was placed into the fixed-bed reactor. The adsorbent was supported by cotton wool. Before each CO_2 adsorption test, the adsorbent was heated to 100 °C for 90 min in N_2 stream at a flow rate of 100 ml/min. After cooling to the desired adsorption temperature, the gaseous mixture containing 85 vol.% N_2 and 15 vol.% CO_2 at the desired flow rate was introduced and passed through the adsorbent. The glass flow meters were used to control the flow rates of the gaseous mixture. The CO_2 concentration of gaseous mixture of the fixed-bed reactor outlet was recorded with an online gas analyzer. The integral equation of the adsorption

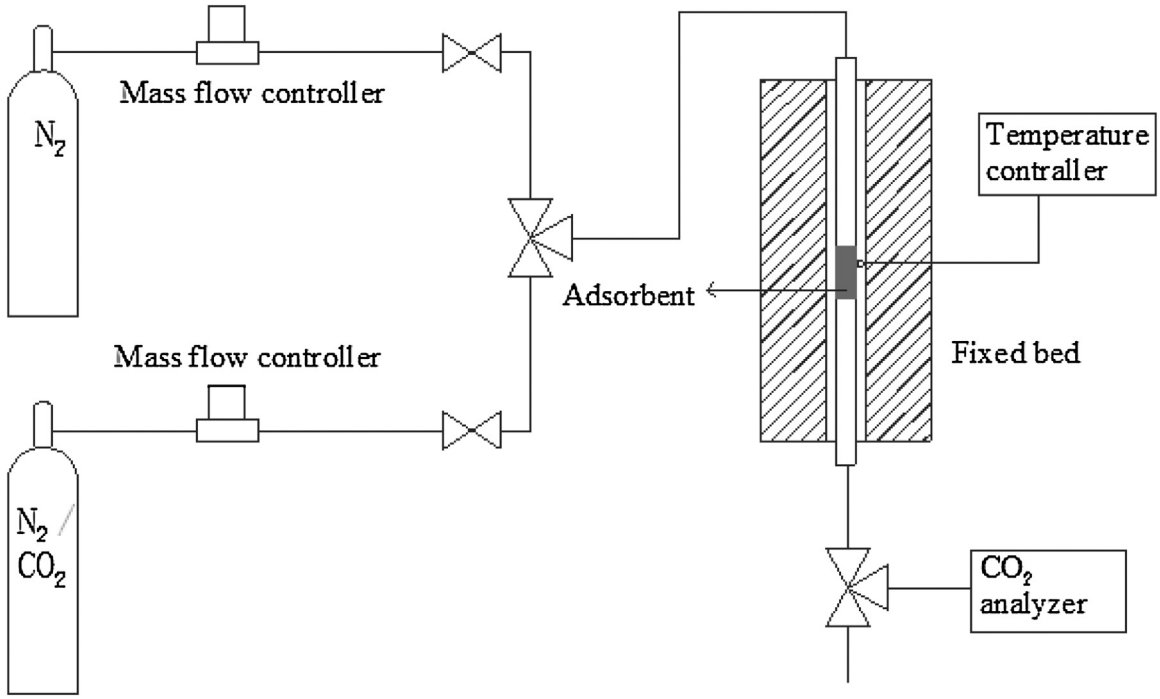

Fig 1. The schematic diagram of fixed bed reactor for the CO_2 capture.

capacity of CO_2 is showed in Eq. (2):

$$q = \frac{Q \times \int_0^t (C_0 - C)dt}{W} \quad (2)$$

where q is the adsorption capacity of CO_2 over the adsorbents (mmol/g); Q represents the influent rate of the gaseous mixture (ml/min); t represent adsorption time (min); W represent adsorbent weight (g); C_0 and C represent the CO_2 concentrations of the inlet and outlet of fixed-bed reactor, respectively. Q_s is defined as the CO_2 saturated adsorption capacity when C is equal to C_0, while breakthrough adsorption capacity (Q_b) is defined as the CO_2 adsorption capacity when C is equal to five percent of C_0; the time corresponding to the breakthrough adsorption capacity is called the breakthrough time.

Results and discussions

Characterization of HPS and HPS-TEPA

The morphology of hierarchical porous silica can be observed in SEM and TEM images in Fig. 2. The special ch structure of HPS consists of the interparticle larger mesoporous and intraparticle wormlike mesoporous. The larger mesoporous should be formed probably thanks to the voids among the aggregated nanoparticles under the conditions of polyethylene glycol presence, the smaller mesoporous in the particles are shaped on account of the function of CTAB template [35].

The isotherms of N_2 adsorption–desorption and distributions of pore size for HPS and MCMC-41 are shown in Fig. 3. Notably, the HPS showed a type IV N_2 adsorption isotherm. This isotherm indicated the porous structure of the materials. The isotherm of HPS exhibits two significant ascents. The first one at a lower relative pressure range gives a relatively pore-size distribution in the range of 2–4 nm, with one sharp peak centered at 2.8 nm with high uniformity. The second ascent point with pronounced capillary condensations at relative pressure of 0.8–0.98 indicated the existence of the large mesoporous channels, corresponding to a large pore-size distribution in the range of 15–40 nm [36,40]. However, for MCM-41, a type IV N_2 adsorption isotherm with H1 hysteresis loops is observed at relative pressure of 0.2–0.4, indicating the single mesoporous structures with facile pore connectivity. Hence, by combining Fig. 3a, b together to give a comparison, we can explain that the material exist hierarchical pore structure with two different pore-size distributions, agree well with the SEM and TEM results. With this special structure, the hierarchical pore structure and larger pore volume of this carrier make it possible to enhance amines loading capacity and provide easier access to the active sites. The resistance for CO_2 diffusion can also decrease in the channel and the corresponding mass transfer rate of CO_2 would increase.

The isotherms of N_2 adsorption/desorption and the corresponding distributions of pore size for before and after amines modified HPS are shown Fig. 4. For amines modified HPS, with increasing TEPA loading capacity, the N_2 adsorption capacity of adsorbent reduce greatly, indicating the corresponding surface area and pore volume of adsorbent reduce. Although a large number of TEPA was loaded in the support, some adsorbents still remain mesoporous structure. This phenomenon was testified by the isotherms of HPS-TEPA-50% and HPS-TEPA-60% which still has a hysteresis loops. These obvious phenomenons also correspond with the distribution of pore-size in Fig. 4(b). Textural properties parameters of before and after amines modified HPS are summarized in Table 1. And the same structure parameter of some order mesoporous materials was also list for comparison in Table 2 [41–43].

For the blank sample, the N_2 adsorption isotherm gives a Brunauer–Emmett–Teller (BET) surface area of 978.7 m^2/g and a larger total pore volume of 2.19 cm^3/g. This pore volume is much larger than the ordered porous silica material, such as MCM-41, SBA-15. What's more, the surface area of the HPS and these order mesoporous materials is about the same. Therefore, the HPS with different pore distribution not only provide a great surface area but a large pore volume. When the HPS was utilized to load the organic amine for CO_2 capture, it is not easy to cause channel blockage and the amount of TEPA can be improved effectively [41–43]. By observing the average pore size, an interesting phenomenon is

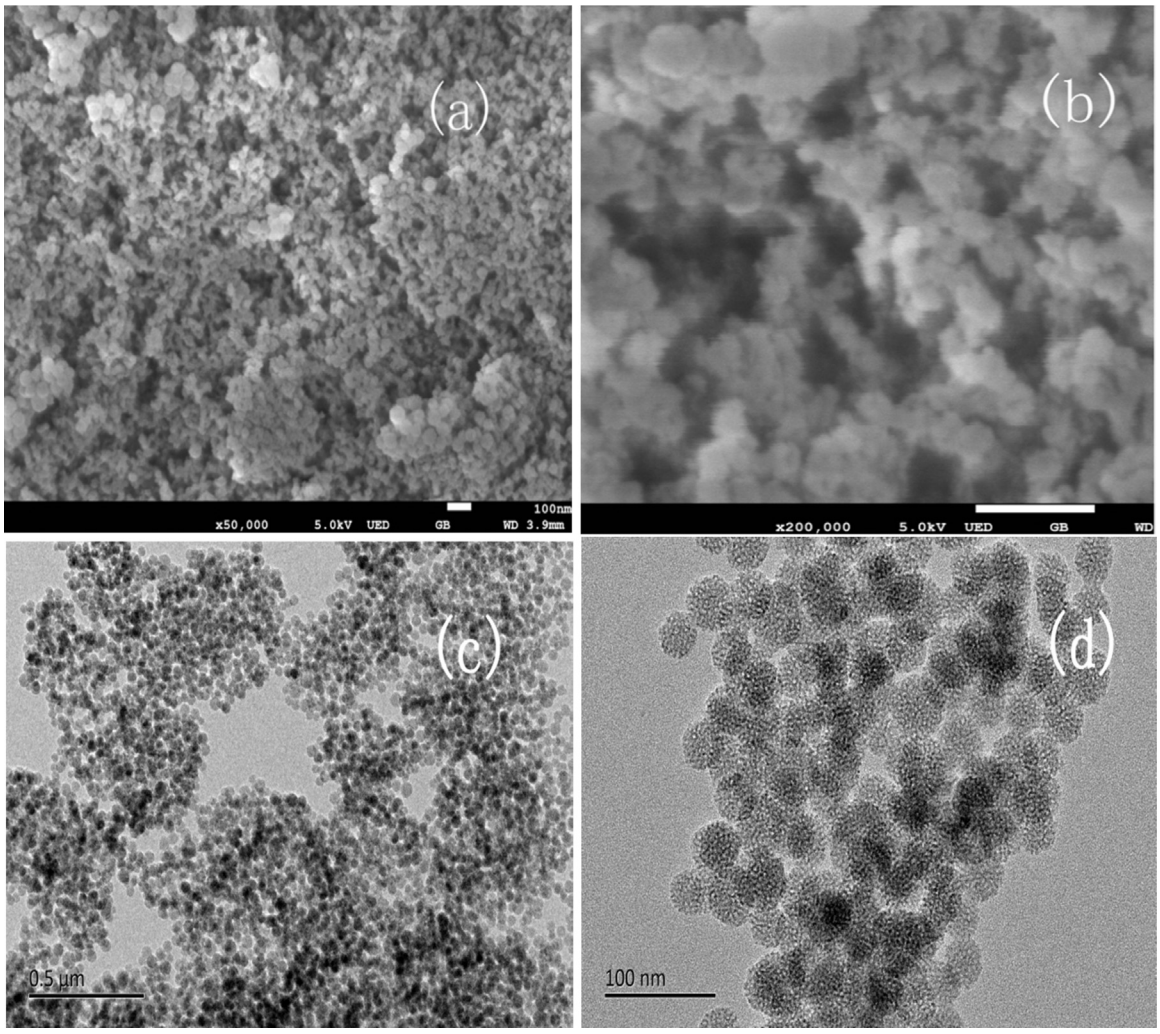

Fig. 2. SEM (a, b) and TEM (c, d) images of the HPS.

found that with the increase of TEPA loaded capacity, the average pore diameter increases. This phenomenon might be contributed to the fact that with the increase of TEPA loaded amount, the small size pores of HPS were firstly filled by the TEPA molecules, so the small size pores were first to be block aged, but some large pores were still remained [44]. Thus, when the pore volume decreases, the average pore size increases. When the loading capacity of TEPA was further raised to 60 wt.%, the adsorbent has only surface area of 20.32 m^2/g. And even there is almost no volume can be tested for the HPS-TEPA-70%, this means that the occurrence of significant pore blockage and the decrease of average pore diameter, just as the HPS-TEPA-70% shows in Table 1.

The analysis of nitrogen content of adsorbents is also shown in Table 1. For the adsorbents with different TEPA loadings, with the increase of TEPA loading amount, the nitrogen content of the adsorbents also increased. Nitrogen content was 12.12 wt.%, 15.59 wt%, 17.73 wt% and 19.94 wt.%, with an increase of TEPA load capacity to 40, 50, 60 and 70 wt.%, respectively. But the amine efficiency of adsorbents did not have the same law. The amine efficiency was 0.375, 0.386, and 0.396 mol CO_2/mol N, with an increase of TEPA load capacity to 40, 50, and 60 wt. %, respectively. When the TEPA load capacity was further increased to 70 wt. %, the amine efficiency was decreased to 0.279 mol CO_2/mol N. It indicated that the HPS-TEPA-60% had the maximum amine efficiency. These trends are in accordance with the CO_2 adsorption capacity. When the TEPA loading exceeds 60 wt.%, since the excessive TEPA hinders the CO_2 diffusion across the TEPA organic layer resulting in many active sites cannot in contact with CO_2 molecules.

Fig. 5 provides XRD patterns for HPS adsorbents modified with different amounts of TEPA. For the HPS, the diffraction patterns only exhibited a relatively broad hump. This phenomenon is most likely thanks to the truth that the carrier are not hydrothermal crystalline on the atomic level in the process of synthesis. So, we cannot observe the reflections at higher angles [38]. The XRD patterns of MCM-41 exhibit four peaks. These peaks are very obvious and the diffraction intensity is very high. These characteristic peaks show that synthetic MCM-41 has a highly ordered structure. So compared with the ordered mesoporous structures of MCM-41, HPS is a material with poor structural order. But it possesses a larger amount of CO_2 capture as the amine impregnated adsorbent by comparison to other amino adsorbent with a ordered mesoporous structures. This is thanks to the support has higher pore volume and hierarchical porous structure observed in BET analysis. The patterns of HPS-TEPA-40% and HPS-TEPA-50% show the same diffraction broad hump, but their intensities especially decrease as the TEPA loaded capacity is increased. This reduction is more prominent for 70%, the diffraction peak disappears. The diffraction intensities can be associated with the scattering contrast between the silicate channel walls and the channel interior [45]. The more TEPA is introduced in the support channels, the weaker diffraction peak intensity between the channel walls and the channel interior of the

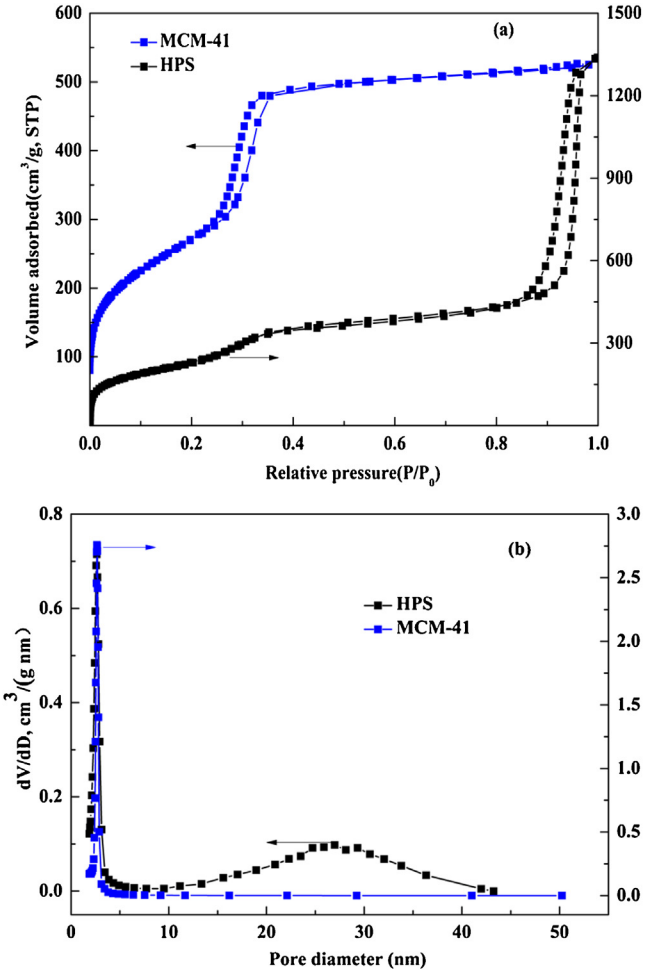

Fig. 3. (a) N_2 adsorption–desorption isotherms and (b) pore size distributions of MCM-41 and HPS.

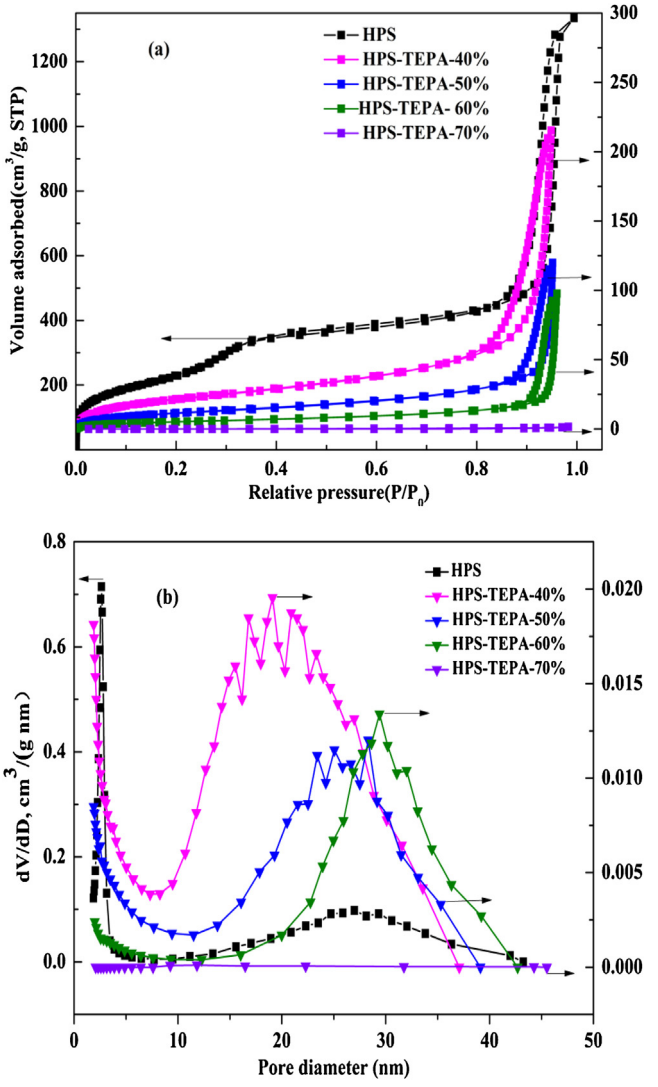

Fig. 4. (a) N_2 adsorption–desorption isotherms and (b) pore size distributions of HPS and adsorbents impregnated with different TEPA content.

material. Similar conclusions were also reported by Qi et al. [46] and Le et al. [39]. And with an increase of amine loaded capacity, more and more channel would collapse leading to decrease of specific surface area and pore volume of adsorbent [28]. These results indicate that amine was successfully impregnated into the HPS.

Fig. 6 provide the FT-IR characterizations for HPS and adsorbents modified with different mass fraction TEPA. For the before and after TEPA modification HPS, wave numbers at 459 cm^{-1}, 814 cm^{-1}, and 1081 cm^{-1} have a relationship with the bending vibration, symmetric stretching vibration and asymmetric stretching vibration of Si—O—Si bond [28,40]. For adsorbents modified with different mass fraction TEPA, wave numbers at 1231 cm^{-1}, 1312 cm^{-1} and 3348 cm^{-1} are connected with the stretching vibration of C—N, the bending vibration of N—H from the secondary amine (N(R)H) in TEPA, respectively [28,47]. Wave numbers at 2922 cm^{-1} and 2834 cm^{-1} are due to the symmetric and non-symmetric stretching vibrations of –CH in TEPA [48]. The new bands at 1570 cm^{-1}, 1470 cm^{-1} correspond to the symmetric and non-symmetric stretching vibrations of N—H in the primary amine ($-NH_2$) in TEPA, indicating that TEPA was successfully impregnated into the HPS. With increasing TEPA impregnation capacity, the characteristic peaks intensity also enhance, indicating that more and more amines are filled into the carrier channels. These observations above suggested that the designed composite sorbents have been successfully prepared.

Table 1
The textural properties, nitrogen content and CO_2 adsorption properties of the HPS and adsorbents impregnated with different TEPA content.

Sample	BET (cm^2/g)	Total pore volume (cm^3/g)	Average pore diameter (nm)	[a]N content (wt%)	CO_2 capture capacity (mmol/g)	Amine efficiency (mol CO_2/mol N)
HPS	978.7	2.19	7.41	0	0.56	–
HPS-TEPA-40%	83.59	0.33	12.81	12.12	3.25	0.375
HPS-TEPA-50%	44.69	0.18	14.00	15.59	4.3	0.386
HPS-TEPA-60%	20.32	0.15	22.56	17.73	5.01	0.396
HPS-TEPA-70%	0.11	0.0025	10.2	19.94	4.03	0.279

[a] Nitrogen content measured by elemental analysis.

Table 2
The comparison of textural properties between the HPS and some order mesoporous support.

Sample	BET (m^2/g)	Total pore volume (cm^3/g)	Average pore diameter (nm)	Refs. [41–43]
HPS	978.7	2.19	7.41	This study
MCM-41	919	0.83	2.97	This study
MCM-41	1088	0.83	2.6	Loganathan et al., 2016
PE-MCM-41	894	1.28	5.1	Loganathan et al., 2016
SBA-15	720	1.20	8.9	Sanz-Pe'rez et al., 2016
PE-SBA-15	428	1.18	15.2	Sanz et al., 2013

CO_2 capture

The influence of TEPA loaded amount

The influence of the TEPA loaded capacity of HPS on the CO_2 adsorption performance has been investigated at 75 °C with a N_2 stream containing 15 vol.% CO_2. And the experiment was carried out at atmospheric pressure which is important to be considered that the flue gases on the commercial scale are released at this pressure.

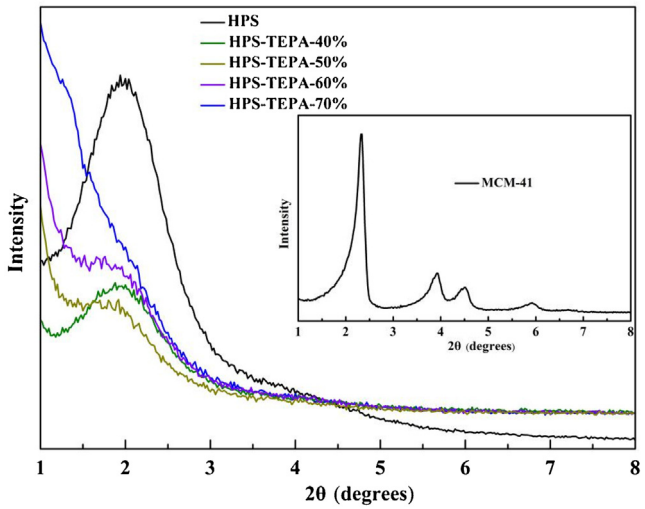

Fig. 5. X-ray diffractograms for MCM-41, HPS and adsorbents impregnated with different TEPA content.

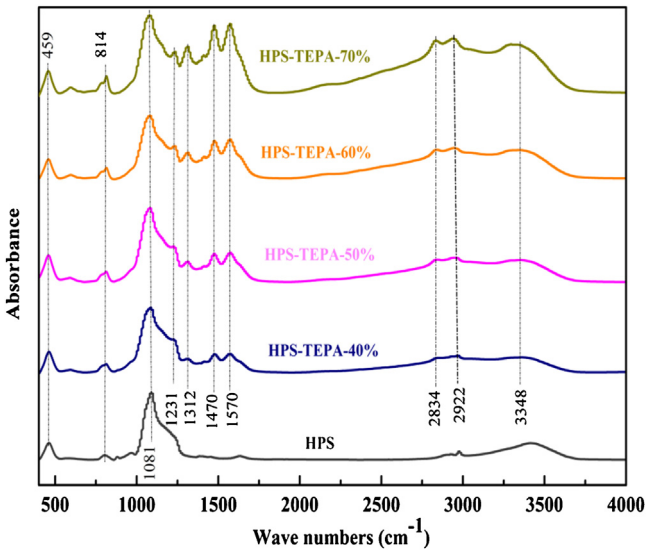

Fig. 6. FT-IR spectra of the HPS adsorbents with different TEPA loadings.

The CO_2 adsorption performance is shown in Fig. 7. For the TEPA modified MCM-41system, CO_2 adsorption capacity was 2.17, 2.6, and 3.01 mmol/g, with an increase of TEPA load capacity to 30, 40, and 50 wt.%, respectively. When the TEPA load capacity was further increased to 60 wt.%, the amount of CO_2 capture decreased to 2.49 mmol/g. It indicated that MCM-41-TEPA-50% had the maximum adsorption capacity.

However, for the TEPA modified HPS system, it exhibited a maximum CO_2 adsorption capacities of 5.01 mmol/g when 60 wt.% TEPA loaded inside pores without overflow. In comparison to TEPA modified adsorbent with a single pore structure, the TEPA modified HPS has a higher CO_2 captured capacity (Table 3) [28,49–53]. The higher CO_2 adsorption capacity of TEPA modified HPS system is due to the large pore volume which can have a larger TEPA oaded capacity, and the different pore diameter which effectively reduce the mass transfer resistance and provide a more effective transportation for CO_2 to the adsorption sites introduced in the adsorbent channel [34].

Further increasing the TEPA loading to 70% for HPS, the CO_2 adsorption capacity decreased to 4.03 mmol/g. Although a higher quantity of TEPA loaded into support can provide more active sites, it also can make the reduction of CO_2 adsorption capacity. This is due to the overmuch TEPA was loaded into the channel or coated outside HPS surface, leading to pore blockage and the great decrease of the interface area between the gas and sorbent, reducing the accessibility of CO_2 molecules to the internal active sites [44,54]. The gel-like morphology of HPS-TEPA-70% is the obvious evidence. Because other adsorbents with less TEPA impregnation capacity have a dry surface after vacuum dry. For the MCM-41 as the support, however, this phenomenon of gel-like morphology of adsorbent occurs when the TEPA loading just to

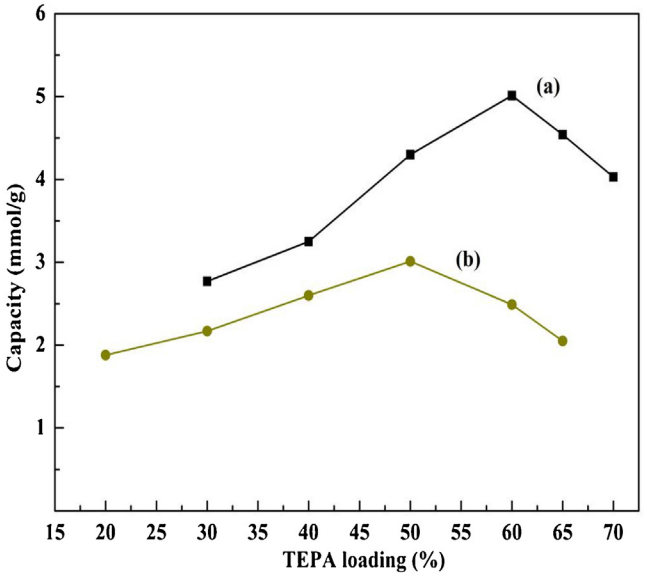

Fig. 7. Comparison of CO_2 sorption capacities with amine loading levels: (a) TEPA modified HPS; (b) TEPA modified MCM-41.

Table 3
Summary of CO_2 adsorption performance using HPS as compared to other TEPA impregnated adsorbent materials.

Adsorbent	CO_2 concentrations (%)	Temp. (°C)	Test mode	Sorption capacity mmol/g	Refs. [28,42,49–53]
HPS-TEPA-40%	15	75	Fixed-bed	3.25	This study
HPS-TEPA-50%	15	75	Fixed-bed	4.30	This study
HPS-TEPA-60%	15	75	Fixed-bed	5.01	This study
HPS-TEPA-70%	15	75	Fixed-bed	4.03	This study
MCM-41-TEPA-50%	15	70	Fixed-bed	2.25	Wang et al., 2015
MSU-1-TEPA-50%	10	75	Fixed-bed	3.87	Wang et al., 2011
MCM-41-TEPA-60%	15	70	Fixed-bed	2.45	Wang et al., 2015
MCM-41-TEPA-60%	100	75	TGA	4.00	Ye et al., 2008
SBA-15-TEPA-60%	10	75	Fixed-bed	3.56	Sanz-Pe'rez et al., 2016
KIT-6-TEPA- 60%	10	60	GC	3.20	L. Sravanthi et al., 2015
MCF-TEPA-70%	10	75	MS	4.34	Feng et al., 2013
Silica gel-TEPA-80%	10	75	Microbalance	3.50	Linneen et al., 2013

Table 4
The breakthrough time and CO_2 adsorption capacity of adsorbents with different TEPA loadings.

Samples	Breakthrough time (min)	Breakthrough adsorption capacity (mmol/g)	Saturated adsorption capacity (mmol/g)
HPS	0	0	0.56
HPS-TEPA-40%	13	2.8	3.25
HPS-TEPA-50%	18	3.83	4.30
HPS-TEPA-60%	20	4.19	5.01
HPS-TEPA-70%	17	3.68	4.03

50%. It is clearly confirmed that the HPS with excellent structural performance can be as a better support material for the impregnation of TEPA to capture CO_2.

The CO_2 capture capacities (both breakthrough and saturated adsorption capacity) of adsorbents with different TEPA loading amount are listed in Table 4. Each adsorbent can achieve the balance of adsorption in a short time after achieving breakthrough adsorption, which can be attributed to the fast kinetics of the adsorption process and small mass transfer resistance of the CO_2 in the adsorbent. The HPS without TEPA modification presented no breakthrough and low adsorption capacity. After modification with TEPA, the breakthrough time and adsorption capacity notably increased compared with blank HPS. With the increase of TEPA loading, the CO_2 adsorption capacity and breakthrough time both increased. But when the TEPA exceeded 60%, the breakthrough time and CO_2 adsorption capacity would decreased, explained as described above by the introduction of more TEPA into the HPS carrier providing more active sites for CO_2 capture. However, with a further increase of TEPA loading amount, TEPA aggregated in the channel or coated outside HPS surface, leading to pore blockage and the increase of CO_2 diffusion resistance to react with active sites in the pores. Among the prepared TEPA modified adsorbents, HPS-TEPA-60% presented optimal breakthrough time and saturated adsorption capacity, and the value was 20 min with 5.01 mmol/g. Moreover, the breakthrough adsorption amount of HPS-TEPA-60% exceeds 80% of the saturated adsorption amount. So the efficient CO_2 capture can be realized by using this adsorbent in commercial applications.

The influence of capture temperature

The influence of temperature on the CO_2 capture process was investigated by operating adsorption experiments at 30 °C, 45 °C, 60 °C, 75 °C, 90 °C and 105 °C with a feed flow rate of 60 ml/min on the HPS-TEPA-60% adsorbent.

As shown in Fig. 8, the TEPA modified HPS showed a dependence on adsorption temperature: the amount of CO_2 capture first increased with the increase of temperature to a maximum, then decreased. 4.45 mmol/g was measured at 45 °C and 4.74 mmol/g was measured at 60 °C for HPS-TEPA-60%. With increasing the temperature, the adsorption capacity of CO_2 continued to grow larger and reached its maximum of 5.01 mmol/g at 75 °C. However, the CO_2 capture capacity dropped to 4.72 mmol/g at 90 °C. This experiments result is similar to the previously reported results by Wang et al. [55]. They also observed the best temperature of 75 °C for CO_2 adsorption from a simulated gas stream over PEI/SBA-15 via a fix-bed method.

The temperature-dependent adsorption results indicate that the CO_2 adsorption is a kinetic control process. As the temperature rises, the expansion of TEPA loaded into different pore of the support and the decrease of CO_2 diffusion resistance make a contribution to the increase of CO_2 adsorption capacity [34]. At low temperature, the TEPA is loaded inside the pore as bulk nanoparticles, being only the external active sites of TEPA accessible to CO_2 molecules [56]. And the diffusion of the CO_2 molecules from the surface to the bulk of TEPA is dominated as the main adsorption resistance. The amount of CO_2 capture is poor due to the CO_2 molecular kinetic energy is not able to overcome the diffusion

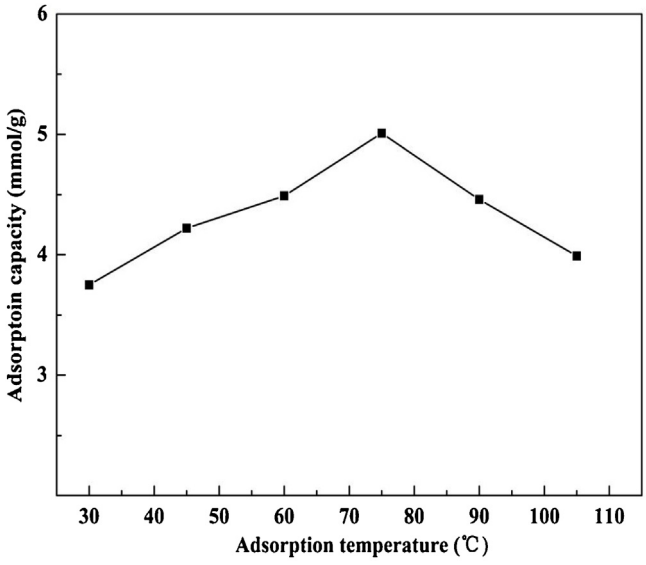

Fig. 8. CO_2 adsorption capacities at different adsorption temperatures.

resistance. When the temperature increase to 75 °C, the TEPA molecule became easier to move and could disperse more uniformly occupying all the available space in the support channel [55,57]. Thus, more active sites were exposed for CO_2 to reaction and the internal diffusion resistance decreased. This leads to a remarkable improvement of CO_2 capture capacity. In contrast, as the temperature rises to 90 °C, although more amine active sites are becoming accessible, CO_2 desorption from adsorption sites in the pore becomes more preferential, leading to a reduce in the CO_2 adsorption capacity. In summary, it is noteworthy that the CO_2 adsorption capacity obtained at 75 °C is very noticeable which makes the TEPA modified HPS materials as good candidates to remove CO_2 effectively by adsorption.

CO_2 adsorption reaction mechanism

In situ infrared (IR) spectroscopy was employed to study the adsorption mechanism over HPS-TEPA-60% adsorbents, as shown in Fig. 9. The nature of adsorbed CO_2 can be revealed by examining relationships among variations of intensities of the NH band at 3298 cm^{-1}, NH_2 at 3365 cm^{-1}, NH_3^+ at 1639 cm^{-1}, C=O at 1685 cm^{-1} from carbamic acid (NCOOH) and O=C=O$^-$ at 1494 cm^{-1} from carbamate ($NHCOO^-$) during CO_2 adsorption [58]. Upon CO_2 adsorption, the intensity of NH_2 at 3365 cm^{-1} decreased while the intensities of NHCOO− at 1494 cm^{-1} and NH_3+ at 3046 cm^{-1} increased. In contrast, the intensities of NH at 3298 cm^{-1} and NCOOH at 1685 cm^{-1} showed a gradual change [59]. The chemically adsorption mechanism can be expressed as follows according to the differences in dynamic behavior of these species.

$$CO_2 + 2RNH_2 \rightarrow RNHCOO^- + RNH_3^+ \quad (3)$$

$$CO_2 + 2R_1R_2NH \rightarrow R_1NCOO^- + R_2NH_2^+ \quad (4)$$

$$CO_2 + R_1NH_2 + R_2NH \rightarrow R_1NH_3^+ + R_2NCOO^- \quad (5)$$

Regenerability of the adsorbent

The large CO_2 capture capacity and better regenerability are necessary for adsorbents in the industrial applications. Ten CO_2 adsorption–desorption cycles were carried out in this study to assess the regenerability of prepared adsorbents by using the adsorbent with the 60 wt.% TEPA loadings as the assessment sample. The CO_2 was adsorbed from the simulated flue gas containing 15% CO_2 and 85% N_2 at 75 °C with the 60 ml/min feed flow rate. And the CO_2 was removed from adsorbent at 100 °C in a pure N_2 stream with 100 ml/min feed flow rate for 90 min. The CO_2 capture capacity of each adsorption–desorption cycles is listed in Fig. 10. After ten times CO_2 adsorption–desorption cycles, the CO_2 capture capacity reduces from 5.01 mmol/g to 4.7 mmol/g, only 6.1% reduction. The results indicated that the HPS-TEPA-60% had better stability and regenerability compared with TEPA impregnated MCM-41 in which CO_2 capture capacity reduced by 7.4% after ten adsorption–desorption cycles reported by Liu et al. [60]. When the MCM-41was modified by TEPA, some single ordered channel are easily blocked leading to a part of TEPA coat the support outer surface. However, for the HPS with different pore distributions, almost all of the TEPA molecules can be dispersed inside the different pore of support, the TEPA was more stably immobilized than that coated outside.

Deactivation model for breakthrough analysis

The CO_2 adsorption reaction of TEPA modified HPS is a gas-solid reaction without catalyst. TEPA molecular would form a relatively thick membranes or bulk in the carrier in the modification process. These membranes or bulk would create diffusion mass transfer resistance during the reaction. And then, these resistances would cause some important changes which could cause a decrease of reaction activity on the solid adsorbent during the reaction process. Aspects of these changes include active surface area, pore structure, reaction rate. As reported in the literature [61–63], the deactivation model could be applied well to such gas-solid reactions. In this model, the influence of all of these factors on the decreasing rate of CO_2 adsorption was combined with a deactivation rate term.

Assumptions: The CO_2 capture process was carried out under the pseudo-steady-state; any mass transfer resistances and the axial diffusion in the reactor are assumed to be negligible. The conservation equation of isothermal species for reactant gas can be described as Eq. (6):

$$-Q\frac{dC}{dW} - k_0 C\alpha = 0 \quad (6)$$

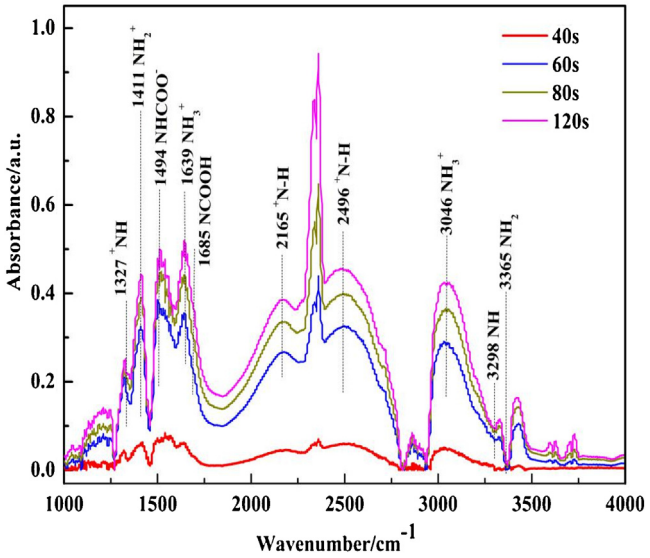

Fig. 9. In situ IR absorbance spectra of the HPS-TEPA-60%.

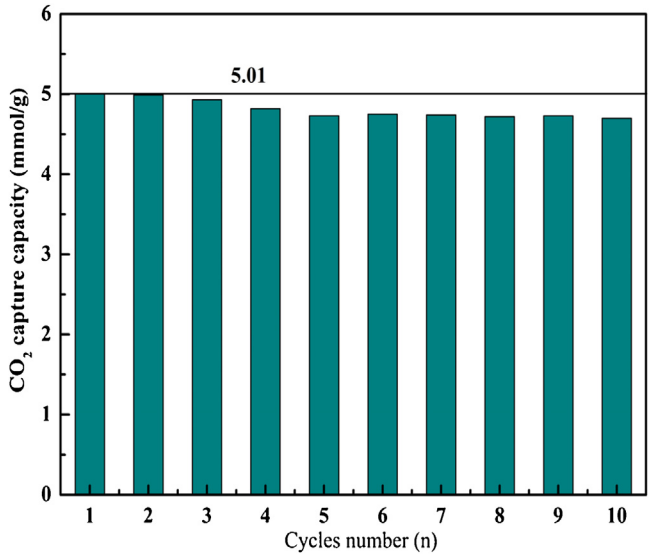

Fig. 10. The cyclic CO_2 adsorption capacity of the HPS-TEPA-60% adsorbent.

The change rate of adsorbent activity equation is described as in Eq. (7) basis on the proposed deactivation model.

$$-\frac{d\alpha}{dt} = k_d C^n \alpha^m \quad (7)$$

The deactivation rate of solid adsorbent is related to the concentration of the reactant gas. Taking n = m = 1 and applying iterative procedure, the above equations can be described as Eq. (8).

$$\frac{C}{C_0} = \exp\left\{\frac{1-\exp\left[k_0\frac{W}{Q}(1-\exp(-k_d t))\right]}{1-\exp(-k_d t)}\exp(-k_d t)\right\} \quad (8)$$

where k_0 represent rate constant of initial sorption (ml/min g), the k_d represent deactivation rate constant (min^{-1}), α represent reaction activity of the adsorbent, and t represent the reaction time.

The result of regression analysis for the measured breakthrough data obtained from the CO_2 adsorption process on modified adsorbents agree well with the deactivation model formula (Eq. (8)). By using a nonlinear regression tool, sorption rate constant k_0 and inactivation rate constant kd can be get through the progress of regression analysis. The correlation parameters (R^2) for the regression analysis of the data under different experimental condition are all higher than 0.99, which indicates a good correlation regression analysis. Therefore, it can be concluded that the deactivation model is very suitable for measured data in the experiment.

The CO_2 adsorption experiments were carry out to study the influence of TEPA loaded capacity on the CO_2 adsorption breakthrough curves. The fitting curves are shown in Fig. 11. By using Eq. (8), the deactivation model and data points measured in the experiment could fit very well for each adsorbent with different TEPA loaded capacity on HPS. The fitting parameters which obtained by the regression analysis between the deactivation model and experimental data are listed in Table 5. With the increase of TEPA loading, the k_0 value also increased. But the values of k_d decreased with increasing TEPA loading. The results showed that HPS-TEPA-60% has the largest amount of CO_2 capture, giving a good agreement with the discussion in Fig. 7.

CO_2 adsorption measurements were carried out at different temperature on HPS-TEPA-60% to test the influence of the adsorption temperature. A better fitting between the data points measured in experiments and deactivation model was gained for each test temperature. With an increase of temperature, the k_0 and k_d were both increased (Table 6). This condition indicated that the adsorption and desorption process of HPS-TEPA-60% were raised. The increase of the molecules activity between CO_2 and amine groups with the increase of temperatures makes the breakthrough curves divert to the right (Fig. 12).

The CO_2 adsorption experiments of HPS-TEPA-60% were performed with different gas flow rates to test and verify the model assumption of neglecting interparticle transport effects. The flow rates of gas mixtures of CO_2 and N_2 were set to 60, 80, 100 ml/min. The breakthrough curves for experiments were gained through the change of CO_2 outlet concentrations with time and they are given in Fig. 13. With the improvement of flow rates for gas mixture, as expected, the breakthrough curves turned to shorter times. The result of regression analysis for deactivation model and data points measured in the experiment is shown in Table 7. As we can see in the table, both k_0 and k_d do not have close relationship with the mixture gas flow rates, which is consistent with the results reported in other literature [61,62].

Table 5
Parameters of the deactivation model for CO_2 adsorption on HPS with different loading amounts.

Samples	k_0 (ml/min g^{-1})	k_d (min^{-1})	R^2
HPA-TEPA-40%	408.9	0.8751	0.9957
HPS-TEPA-50%	413.9	0.6346	0.9971
HPS-TEPA-60%	451.3	0.6234	0.991

Table 6
Parameters of the deactivation model for CO_2 adsorption on HPS-TEPA-60% at different temperatures.

Temperature (°C)	k_0 (ml/min g^{-1})	k_d (min^{-1})	R^2
45	200.7	0.3109	0.9983
60	247.7	0.3711	0.9977
75	451.3	0.6234	0.991

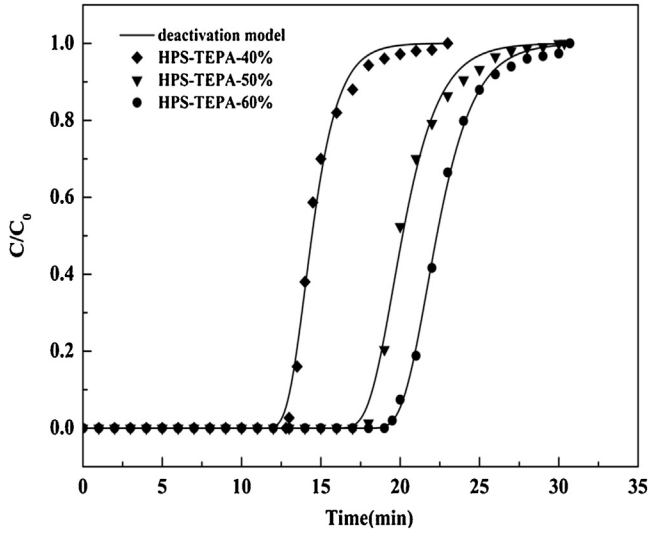

Fig. 11. Comparison of experimental results to the deactivation model for CO_2 adsorption on HPS-TEPA-40%, HPS-TEPA-50%, and HPS-TEPA-60%.

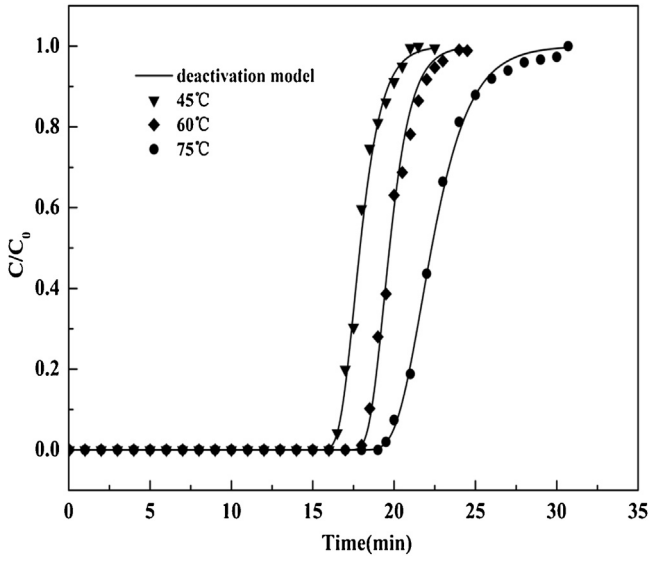

Fig. 12. Comparison of experimental results to the deactivation model for CO_2 adsorption on HPS-TEPA-60% at 45 °C, 60 °C, and 75 °C.

Table 7
Parameters of the deactivation model for CO_2 adsorption on HPS-TEPA-60% at different flow rates.

Q (ml/min)	k_0 (ml/min g^{-1})	k_d (min^{-1})	R^2
60	451.3	0.6234	0.9991
80	436.4	0.6309	0.9988
100	447.2	0.6198	0.9975

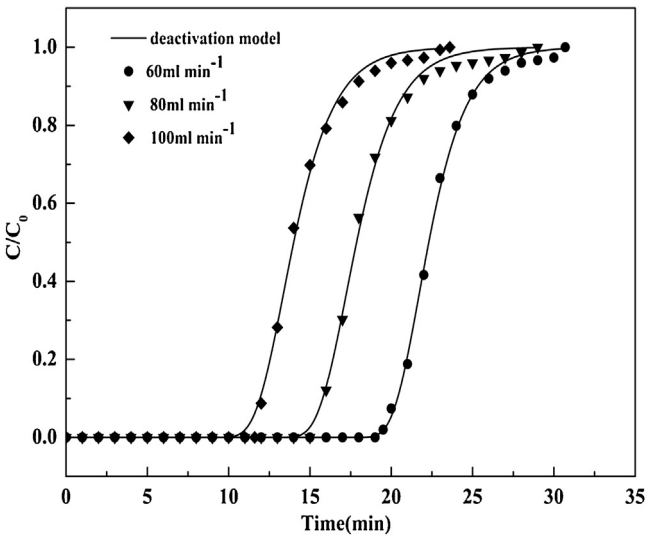

Fig. 13. Comparison of experimental results to the deactivation model for CO_2 adsorption on HPS-TEPA-60% at 60, 80, and 100 ml/min.

Conclusions

In summary, amine modified solid adsorbent for CO_2 capture was developed by HPS impregnated with TEPA. The structure characteristics of HPS with the different pore distribution and the large pore volume formed by the internal mesoporosity and the accumulation of spherical particles had an important influence on the CO_2 adsorption capacity and kinetics. Under the same experiment conditions, the HPS-TEPA-60% exhibited the maximum CO_2 adsorption capacity of 5.01 mmol/g. It has an obvious increase compared with the highest values of 2.49 mmol/g for 60 wt.% TEPA modified MCM-41. Moreover, HPS-TEPA-60% exhibited excellent stability and regenerability by changing the temperature from 75 °C (adsorption) to 100 °C (desorption). When the adsorption experiments were repeated 10 times, the amount of CO_2 capture decreased from 5.01 mmol/g to 4.7 mmol/g, only 6.1% reduction. The deactivation model was successfully used to describe the CO_2 adsorption on TEPA modified HPS under different conditions. Considering the higher CO_2 adsorption capacity and excellent regenerability, amine modified HPS possess great potential for CO_2 capture from the post-combustion flue gas in the future.

Acknowledgments

This work was supported by the National Natural Science Foundation of China (Nos. 21376003,21676174 and U1610115), and the Joint Fund of Shanxi Provincial Coal Seam Gas (2015012019).

References

[1] K.Z. House, C.F. Harvey, M.J. Aziz, D.P. Schrag, Energy Environ. Sci. 2 (2009) 193.
[2] P. Prakash, A. Venkatnathan, RSC Adv. 6 (2016) 55438.
[3] N. MacDowell, N. Florin, A. Buchard, J. Hallett, A. Galindo, G. Jackson, C.S. Adjiman, C.K. Williams, N. Shah, P. Fennell, Energy Environ. Sci. 3 (2010) 1645.
[4] D.W. Keith, Science 325 (2009) 1654.
[5] S.D. Kenarsari, D. Yang, G. Jiang, S. Zhang, J. Wang, A.G. Russell, Q. Wei, M. Fan, RSC Adv. 3 (2013) 22739.
[6] X. Wang, L. Chen, Q. Guo, Chem. Eng. J. 260 (2015) 573.
[7] X. Wang, Q. Gao, T. Kong, Chem. Eng. J. 273 (2015) 472.
[8] S. Wang, S. Yan, X. Ma, J. Gong, Energy Environ. Sci. 4 (2011) 3805.
[9] J. Wang, L. Huang, R. Yang, Z. Zhang, J. Wu, Y. Gao, Q. Wang, D. O'Hareb, Z. Zhong, Energy Environ. Sci. 7 (2014) 3478.
[10] D. Bastani, N. Esmaeili, M. Asadollahi, J. Ind. Eng. Chem. 19 (2013) 375.
[11] O. Cheung, N. Hedin, RSC Adv. 4 (2014) 14480.
[12] C. Chen, S. Kim, W.S. Cho, W.S. Ahn, Appl. Surf. Sci. 332 (2015) 167.
[13] C.H. Lee, D.H. Hyeon, H. Jung, W. Chung, D.H. Jo, D.K. Shin, S.H. Kim, J. Ind. Eng. Chem. 23 (2015) 251.
[14] H.M. Yoo, S.Y. Lee, S.J. Park, J. Solid State Chem. 197 (2013) 361.
[15] J. Wang, L. Huang, Q. Zheng, Y. Qiao, Q. Wang, J. Ind. Eng. Chem. 36 (2016) 255.
[16] R. Sanz, G. Callej, A. Arencibia, E.S. Sanz-Pérez, Microporous Mesoporous Mater. 209 (2015) 165.
[17] S.Y. Lee, S.J. Park, J. Ind. Eng. Chem. 23 (2015) 1.
[18] S. Ahmed, A. Ramli, S. Yusup, Int. J. Greenh. Gas Control 51 (2016) 230.
[19] L. Li, Y. Li, X. Wen, F. Wang, N. Zhao, F. Xiao, W. Wei, Y. Sun, Energy Fuels 25 (2011) 3835.
[20] S.A. Tawfik, X.Y. Cui, S.P. Ringer, C. Stampfl, RSC Adv. 5 (2015) 50975.
[21] D.A. Yang, H.Y. Cho, J. Kim, S.T. Yang, W.S. Ahn, Energy Environ. Sci. 5 (2012) 6465.
[22] Y. Lin, C. Kong, L. Chen, RSC Adv. 6 (2016) 32598.
[23] M. Radosz, X. Hu, K. Krutkramelis, Y. Shen, Ind. Eng. Chem. Res. 47 (2008) 3783.
[24] S. Choi, J.H. Drese, C.W. Jones, ChemSusChem 2 (2009) 796.
[25] R.A. Khatri, S.S.C. Chuang, Y. Song, M. Gray, Energy Fuels 20 (2006) 1514.
[26] Y. Le, D. Guo, B. Cheng, J. Yu, J. Colloid Interface Sci. 408 (2013) 173.
[27] J. Yu, Y. Le, B. Cheng, RSC Adv. 17 (2012) 6784.
[28] X. Wang, L. Chen, Q. Guo, Chem. Eng. J. 260 (2015) 573.
[29] X. Wang, Q. Guo, J. Zhao, L. Chen, Int. J. Greenh. Gas Control 37 (2015) 90.
[30] X. Xu, C. Song, J.M. Andresen, B.G. Miller, A.W. Scaroni, Energy Fuels 16 (2002) 1463.
[31] S. Ahmed, A. Ramlib, S. Yusup, Int. J. Greenh. Gas Control 51 (2016) 230.
[32] R. Ullah, M. Atilhan, S. Aparicio, A. Canlier, C.T. Yavuz, Int. J. Greenh. Gas Control 43 (2015) 22.
[33] G. Chandrasekar, W.J. Son, W.S. Ahn, J. Porous Mater. 16 (2009) 545.
[34] J. Wang, D. Long, H. Zhou, Q. Chen, X. Liu, L. Ling, Energy Environ. Sci. 5 (2012) 5742.
[35] J.H. Smått, S. Schunk, M. Linde'n, Chem. Mater. 15 (2003) 2354.
[36] X.Y. Yang, Y. Li, G. Van Tendeloo, F.S. Xiao, B.L. Su, Adv. Mater. 21 (2009) 1368.
[37] C. Chen, S. Bhattacharjee, Appl. Surf. Sci. 396 (2017) 1515.
[38] S. Loganathan, M. Tikmani, A.K. Ghoshal, Langmuir 29 (2013) 3491.
[39] M.U.T. Le, S.Y. Lee, S.J. Park, Int. J. Hydrogen Energy 39 (2014) 12340.
[40] C. Chen, S.T. Yang, W.S. Ahn, R. Ryoo, Chem. Commun. 24 (2009) 3627.
[41] S. Loganathan, M. Tikmani, A. Mishra, A.K. Ghoshal, Chem. Eng. J. 303 (2016) 89.
[42] E.S. Sanz-Pe'rez, A. Arencibia, R. Sanz, G. Calleja, Adsorption 22 (2016) 609.
[43] R. Sanz, G. Calleja, A. Arencibia, E.S. Sanz-Pe'rez, Energy Fuels 27 (2013) 7637.
[44] K. Li, J. Jiang, S. Tian, F. Yan, X. Chen, J. Mater. Chem. A 3 (2015) 2166.
[45] K.S.N. Kamarudin, N. Alias, Fuel Process. Technol. 106 (2013) 332.
[46] G. Qi, Y. Wang, L. Estevez, X. Duan, N. Anako, A.H.A. Park, W. Li, C.W. Jones, E.P. Giannelis, Energy Environ. Sci. 4 (2011) 444.
[47] W. Klinthong, C.H. Huang, C.S. Tan, Ind. Eng. Chem. Res. 55 (2016) 6481.
[48] Q. Chen, F. Fan, D. Long, X. Liu, X. Liang, W. Qiao, L. Ling, Ind. Eng. Chem. Res. 49 (2010) 11408.
[49] X.R. Wang, H.Q. Li, H.T. Liu, X.J. Hou, Microporous Mesoporous Mater. 142 (2011) 564.
[50] M.B. Yue, L.B. Sun, Y. Cao, Y. Wang, Z.J. Wang, J.H. Zhu, Chem. Eur. 14 (2008) 3442.
[51] Y. Liu, J. Shi, J. Chen, Q. Ye, H. Pan, Z. Shao, Y. Shi, Microporous Mesoporous Mater. 134 (2010) 16.
[52] X.X. Feng, G.S. Hu, X. Hu, G.Q. Xie, Y.L. Xie, J.Q. Lu, M.F. Luo, Ind. Eng. Chem. Res. 53 (2013) 4221.
[53] N. Linneen, R. Pfeffer, Y.S. Lin, Microporous Mesoporous Mater. 176 (2013) 123.
[54] L. Zhang, N. Zhan, Q. Jin, H. Liu, J. Hu, Ind. Eng. Chem. Res. 55 (2016) 5885.
[55] X. Wang, X. Ma, V. Schwartz, J.C. Clark, S.H. Overbury, S. Zhao, X. Xu, C. Song, Phys. Chem. Chem. Phys. 14 (2012) 1485.
[56] R. Sanz, G. Calleja, A. Arencibia, E.S. Sanz-Perez, Appl. Surf. Sci. 256 (2010) 5323.
[57] J. Zhao, F. Simeon, Y. Wang, G. Luo, T.A. Hatton, RSC Adv. 2 (2012) 6509.
[58] W.C. Wilfong, C.S. Srikanth, S.S. Chuang, ACS Appl. Mater Interfaces 6 (2014) 13617.
[59] Y. Zhai, S.S.C. Chuang, Energy Technol. 5 (2017) 354.
[60] Z. Liu, Y. Teng, K. Zhang, Y. Cao, W. Pan, J. Fuel Chem. Technol. 41 (2013) 469.
[61] S. Yasyerli, G. Dogu, I. Ar, Ind. Eng. Chem. Res. 40 (2001) 5206.
[62] Q. Ye, J. Jiang, C. Wang, Y. Liu, H. Pan, Y. Shi, Energy Fuels 26 (2012) 2497.
[63] C. Ji, L. Zhang, L. Li, F. Li, F. Xiao, N. Zhao, W. Wei, Y. Chen, F. Wu, Ind. Eng. Chem. Res. 55 (2016) 7853.